



Deposited via The University of Leeds.

White Rose Research Online URL for this paper:

<https://eprints.whiterose.ac.uk/id/eprint/169498/>

Version: Accepted Version

---

**Article:**

Laurent, H, Baker, DL, Soper, AK et al. (2020) Solute Specific Perturbations to Water Structure and Dynamics in Tertiary Aqueous Solution. *The Journal of Physical Chemistry B*, 124 (48). pp. 10983-10993. ISSN: 1520-6106

<https://doi.org/10.1021/acs.jpccb.0c07780>

---

© 2020 American Chemical Society. This is an author produced version of an article published in *The Journal of Physical Chemistry B*. Uploaded in accordance with the publisher's self-archiving policy.

**Reuse**

Items deposited in White Rose Research Online are protected by copyright, with all rights reserved unless indicated otherwise. They may be downloaded and/or printed for private study, or other acts as permitted by national copyright laws. The publisher or other rights holders may allow further reproduction and re-use of the full text version. This is indicated by the licence information on the White Rose Research Online record for the item.

**Takedown**

If you consider content in White Rose Research Online to be in breach of UK law, please notify us by emailing [eprints@whiterose.ac.uk](mailto:eprints@whiterose.ac.uk) including the URL of the record and the reason for the withdrawal request.

# Solute Specific Perturbations to Water Structure and Dynamics in Tertiary Aqueous Solution

Harrison Laurent<sup>1</sup>, Daniel Baker<sup>1</sup>, Alan Soper<sup>2</sup>, Michael Ries<sup>1</sup>, Lorna Dougan<sup>\*1,3</sup>

<sup>1</sup>Department of Physics and Astronomy, University of Leeds, Leeds, UK

<sup>2</sup>ISIS Facility, STFC Rutherford Appleton Laboratory, Didcot, UK

<sup>3</sup>Astbury centre for Structural and Molecular Biology, University of Leeds, Leeds, UK

Corresponding email address: L.Dougan@leeds.ac.uk

## 1. Abstract

Liquid water is known as the “universal” solvent, capable of dissolving a wide variety of different solutes. While much is now understood about the impact of solutes on water structure in binary solutions, it is much more challenging to deconvolute the potentially competing effects of more complex solutions. Here, we present a correlative NMR and neutron diffraction study to examine the solute induced perturbation of water structure and dynamics in a tertiary solution containing the naturally occurring osmolyte trimethylamine N-oxide (TMAO) and magnesium perchlorate ( $\text{Mg}(\text{ClO}_4)_2$ ). We show that while TMAO and  $\text{Mg}(\text{ClO}_4)_2$  perturb water structure in an opposing manner, the two solutes slow water dynamics in an additive manner. We quantify the relative ability of each solute to perturb water by introducing a weighting parameter, and show that TMAO is 1.54 times more effective at perturbing water structure and dynamics than  $\text{Mg}(\text{ClO}_4)_2$ . The combination of NMR, neutron diffraction and computational modelling offers unprecedented access to the structure and dynamics of more complex aqueous solutions, permitting deconvolution of solute specific perturbation of water. Such insight provides a new route to understand this universal solvent in the context of important and relevant aqueous environments.

## 2. Introduction

Liquid water is fundamental to life on Earth and has been extensively studied to understand its host of unusual properties, such as its expansion upon freezing, its density maximum at 4°C, and its unusually high specific heat capacity, melting and boiling points<sup>1-9</sup>. This “anomalous” behaviour emerges as a result of hydrogen bonds, the electrostatic interaction between the more positively charged hydrogens and the more negatively charged oxygen atom between neighbouring molecules. The molecular properties of water result in diverse structural and dynamical roles in biology, acting as a solvent for a variety of different solutes, as well as a reactant, catalyst, chaperone and controller<sup>10,11</sup>. Indeed, water is essential for life, and interactions with water are a major driving force for biomolecular structure, dynamics and function in living systems, including in protein folding and partitioning of solutes across membranes. To understand living systems, we need an accurate understanding of the structure and dynamics of water in relevant aqueous environments, containing solutes such as salts, osmolytes and biological molecules. However, the properties of aqueous solutions of even the simplest ions result from a subtle balance of geometry, density, hydrogen bonding and charge interactions. This has prompted a range of investigations into bulk measurements of enthalpies, entropies and heat capacities of pure water and changes due to dissolving solutes, as well as studies of hydration of solutes, and solute perturbation of water structure and dynamics<sup>6,7</sup>.

Two powerful methods of investigating water structure are x-ray and neutron diffraction techniques, which are sensitive to the electron cloud and the nuclei of the water molecules respectively<sup>12</sup>. These diffraction techniques allow access to the intermolecular pair correlation function  $g(r)$  of a system, which is related to the probability of finding an atom of a particular type at a given distance from a central atom. Neutrons are extremely sensitive to the nucleus of hydrogen and its isotope deuterium. Therefore, neutron diffraction has been used extensively to study the structure of water and aqueous

systems including those containing ionic compounds<sup>7,13-16</sup>, model biomolecules such as amino acids and peptides<sup>17-26</sup>, protecting and denaturing osmolytes<sup>27-30</sup>, and alcohols<sup>31-35</sup>. These studies have helped us to better understand the influence that these solutes have on the structure of water both in their hydration shells and in the bulk. They have also revealed information about the thermodynamics of self-association and segregation of solutes in aqueous solution<sup>27,28,31,32,34,35</sup>, such as the excess entropy of mixing in alcohol solutions<sup>33</sup>, details of the local solute-water conformations around amino acids and peptides that are potentially crucial in the early stages of protein folding<sup>17-24,26,30</sup>, and potential mechanisms underlying Hofmeister and pressure-like effects<sup>7,13-16,30</sup>.

Nuclear Magnetic Resonance (NMR)<sup>36-38</sup> is a technique which has been widely applied for the study of aqueous solutions and biological macromolecules<sup>6,7,39-51</sup>. This allows for the extrapolation of information such as the relative abundance of isomers, macromolecular structure, rotational motions, diffusion, and perturbations to the strength of hydrogen bonds present in the system. It also allows for water in aqueous systems to be studied in detail, as hydration water and bulk water have separate peaks in <sup>17</sup>O NMR<sup>44</sup>. This methodology has been successfully applied to ions in solution, including Mg(ClO<sub>4</sub>)<sub>2</sub>, to determine the rotational dynamics, coordination number, and residence times of water molecules in the ionic hydration shell<sup>45</sup>. It has also been applied to alcohols, diols, amines, diamines<sup>50,52</sup>, denaturants such as guanidine and alkylated urea<sup>41</sup>, and noble gasses<sup>53</sup> in solution to observe perturbations to hydrophobic hydration dynamics in response to pressure, temperature, or proximity to a polar group. These studies also helped demonstrate a correlation between entropy of hydration, and partial molar volumes and partial molar heat capacities at infinite dilution with dynamic hydration number<sup>50</sup>.

While neutron diffraction and NMR studies of binary aqueous solutions containing one solute species are now plentiful, there have been relatively few attempts to examine more complex aqueous solutions. In biological systems the water is not bulk liquid water. For example, measurements of water dynamics in the cell suggest that 10-25% of water molecule have slower reorientational dynamics, by an order of magnitude, than those in the bulk<sup>2,54-56</sup>. The cytosol or intracellular fluid consists of water (~80%) and dissolved ions, small molecules such as osmolytes and larger biomolecule such as proteins. How can we begin to understand the structure and dynamics of water in these complex solutions?

A first step is to deconvolute the solute induced perturbation of water structure and dynamics in tertiary aqueous solutions. Notable recent examples of tertiary aqueous solutions are studies containing trimethylamine N-oxide (TMAO) and either urea<sup>28</sup> or magnesium perchlorate (Mg(ClO<sub>4</sub>)<sub>2</sub>)<sup>57</sup> as a second solute. TMAO is a naturally occurring osmolyte that stabilises proteins against the denaturing effects of other solutes, pressure, and temperature<sup>58</sup>. Conversely Mg(ClO<sub>4</sub>)<sub>2</sub> has been shown to compress water structure in a manner similar to a large external pressure<sup>13</sup>. Given TMAO's action as a protecting osmolyte under pressure, we recently investigated if TMAO was capable of restoring the hydrogen bonded network of water against the perturbation induced by Mg(ClO<sub>4</sub>)<sub>2</sub> using neutron diffraction and an established computational modelling tool, empirical potential structure refinement (EPSR)<sup>57</sup>. This study revealed that TMAO was indeed capable of partially restoring the hydrogen bonded network of water, as evidenced by the position of the coordination shells and height of the first peak in the water oxygen-oxygen  $g(r)$ , and the average interaction energy between two hydrogen bonded water molecules. However, while neutron diffraction can provide powerful insights into liquid structure it provides no access to water dynamics.

The importance of considering both these aspects when studying aqueous solutions becomes clear if we consider studies on potassium halides. Neutron scattering data and computational modelling on aqueous potassium halides shows that both KI and KF perturb water structure in a very similar manner<sup>15</sup>, with the 2<sup>nd</sup> peak in the water oxygen-oxygen  $g(r)$  moving inwards to shorter distances, indicating a more compressed structure. This is also shown in H<sup>1</sup> NMR peak shift data (Fig S1), where KF, KCl, KBr, and KI all result in a shift of the H<sup>1</sup> NMR peak of water to lower ppm, indicative of weakened

hydrogen bonding between water molecules. However molecular dynamics and NMR studies on KF and KI clearly show that while KF retards water dynamics, KI accelerates water dynamics<sup>47</sup>. These two salts could therefore be considered very similar or very different if only their structural or dynamic perturbations to water are considered. The importance of considering both aspects also extends to hydrophobic biological macromolecules as described earlier, where parameters such as the dynamic hydration number require both structural and dynamic information. Therefore, for a full understanding of solute induced perturbation of water both structural and dynamic information is required.

Here we combine NMR data with further analysis of neutron diffraction data to demonstrate a powerful correlative approach which deconvolutes solute perturbation of water structure and dynamics. We show that while TMAO and  $\text{Mg}(\text{ClO}_4)_2$  act to perturb water structure in an opposing manner, with each solute effectively “cancelling the other out”, they instead act to perturb water dynamics in an additive manner. We demonstrate a quantitative approach for determining the relative perturbative action of each solute by forming a single master curve of the data using a weighting parameter. This correlative approach helps bridge the gap between important yet simple model systems, such as binary solutions, and more complex solutions that are towards “real world” systems in which organisms and biomacromolecules reside and function.

### 3. Methods

#### a. NMR sample preparation

Aqueous TMAO and  $\text{Mg}(\text{ClO}_4)_2$  samples were prepared by first dissolving  $\text{Mg}(\text{ClO}_4)_2$  or TMAO dihydrate, obtained from Sigma-Aldrich and used without further purification, to 2.0 mol/kg  $\text{H}_2\text{O}$  in ultrapure water. These were then combined in appropriate ratios with ultrapure water to yield every possible combination of 0-1.0 mol/kg  $\text{H}_2\text{O}$  in 0.2 mol/kg  $\text{H}_2\text{O}$  increments for mixed TMAO  $\text{Mg}(\text{ClO}_4)_2$  solutions, yielding 36 samples in total. The samples were then placed in 5 mm borosilicate NMR tubes (Fluorochem Ltd) for NMR data acquisition. The NMR tubes also contained 1 mm sealed borosilicate x-ray tubes containing dimethyl sulfoxide (DMSO - Sigma-Aldrich) to serve as a calibration peak as DMSO shows a strong single peak at 2.50 ppm<sup>38</sup> in  $^1\text{H}$  NMR measurements. All data were taken at 27°C.

#### b. NMR spectral acquisition

$^1\text{H}$  NMR spectra were acquired using a Bruker Avance II 400 MHz NMR spectrometer. Stronger hydrogen bonds result in deshielding of the hydrogen proton, and therefore the observed NMR peak for water hydrogen is shifted downfield (to higher ppm). The origin of this affect remains unclear, likely due to inadequacies in defining hydrogen bonding itself. The traditionally adopted explanation is that a stronger hydrogen bond causes the hydrogen atom on a water molecule to move further away from its host molecule. It therefore experiences less shielding from the electrons located within the OH bond and the spin on the proton precesses with a higher frequency, causing a downfield shift. However, as distance is strongly affected by quantum effects, there is no simple rule between force field strength and distance. It is more likely to result from distortion of the force field in which the proton sits, causing vibrational and rotational frequencies to shift. Peak shift data can therefore be considered an indicator of structural perturbations to the water network<sup>36-38</sup>.

Proton NMR relaxometry  $T_1$  data were acquired using a Magritek Spinsolve 43 MHz NMR spectrometer (Magritek) via inversion recovery.  $T_1$  relaxation occurs following the application of the 180° pulse that inverts the net magnetization of the spins present in the sample, which were initially aligned parallel to the large external magnetic field (z-axis). As the molecules then translate and rotate in solution the spins experience varying time-dependent local magnetic fields due to interactions with other spins. The spectral density of these fluctuations, at the Larmor frequency ( $\omega$ ) and twice the Larmor frequency, determine the spin-lattice relaxation rate<sup>36-38</sup>. The characteristic time period for the spins to

return to equilibrium is described by the time constant  $T_1$  shown in equation 1, where  $M_z(t)$  is the nuclear spin magnetization in the z direction at a time  $t$ . Example data shown in Fig S2.

$M_z(t) = M_z(0) \left( 1 - 2e^{-\frac{t}{T_1}} \right)$	(1)
--	-----

As the spectral density of the time-varying magnetic field experienced by a spin depends on the rotational motion of the molecule, the  $T_1$  decay time is also dependent on rotational motion. It can be shown that in the fast limit ( $\omega\tau_{RCT} \ll 1$ ),  $T_1^{-1} \propto \tau_{RCT}$ , where  $\tau_{RTC}$  is the rotational correlation time of the molecule, roughly equal to the time taken for the root-mean-square deflection of the molecule to be approximately one radian<sup>36,38,46</sup>. It therefore serves as a measure of the microscale dynamics of the system, where accelerated dynamics would correspond to a lower  $T_1^{-1}$ , and can be used to study changes to the rotational correlation time of the water molecules in the system.

#### c. NMR diffusion

The diffusion coefficient  $D$  for the water molecules in each sample was determined using a Bruker Avance II 400 MHz NMR spectrometer. This is done using the principle of pulsed field gradient spin echo<sup>37</sup>. In addition to the uniform large static external magnetic field parallel to the z axis, a magnetic field gradient  $G$  of increasing magnitude is also applied parallel to the z axis. The Larmor frequency of the individual spins in the sample is therefore dependent on their location in the z direction, which enables diffusion measurements to be carried out.

If one measures signal attenuation as a function of field gradient  $G$ , one can use the Stejskal-Tanner expression<sup>59</sup>, shown in equation 2 where  $I_G$  is the signal at gradient strength  $G$ ,  $\gamma$  is the gyromagnetic ratio of the nuclei in question, in our case hydrogen,  $\delta$  is the length of the gradient pulses, and  $\Delta$  is the diffusion period between gradient pulses, to extract the diffusion coefficient  $D$ .

$I_G = I_{G=0} \exp \left[ -(\gamma\delta G)^2 D \left( \Delta - \frac{\delta}{3} \right) \right]$	(2)
--	-----

#### d. Neutron scattering

The acquisition of neutron diffraction data and subsequent analysis for mixed aqueous  $\text{Mg}(\text{ClO}_4)_2$  TMAO is previously described<sup>57</sup> and will therefore only be briefly overviewed here. Diffraction data were taken using the Near to Intermediate Range Order Diffractometer (NIMROD)<sup>60</sup> and corrected for multiple scattering, attenuation, and inelasticity effects using Gudrun<sup>12</sup>. Three isotopic variants of water and three isotopic variants of TMAO were used to help deconvolute the total interference scattering cross section produced by Gudrun. Full details of the neutron diffraction can be found in the Methods section of our recent study<sup>57</sup>. A complete list of samples is available in the supporting information (List S1).

#### e. Empirical potential structure refinement

The scattering data were analysed using empirical potential structure refinement (EPSR) as described previously<sup>57</sup>. This is a Monte Carlo based analysis tool which equilibrates a simulated box of molecules that is representative of the experimental sample using a reference potential containing a Lennard-Jones and a Coulomb component, and then applies an empirical potential to refine the simulation against the experimental scattering data<sup>61,62</sup>. The result is a simulated box of molecules whose structure (or atomic arrangement) is consistent with the experimental scattering data. It is important to note here that EPSR does not guarantee a unique structure, merely one that is consistent with the scattering data. The resulting simulated box can then be used to calculate pair correlation functions ( $g(r)$ s) and coordination

numbers, as well as more detailed analysis such as hydrogen bond energies and conformations as detailed in section 3(g). The simulation parameters for the reference potential, as well as the fits to the scattering data, are available in the supporting information (Table S1, Table S2, Fig S3).

#### f. Hydrogen bonding analysis

The simulated box of atoms produced by EPSR can be analysed further using a hydrogen bond analysis code. Since its first implementation<sup>57</sup> it has been expanded here to study hydrogen bonding in more detail as described below. The hydrogen bond analysis code first reads in the coordinates for all the simulated molecules. Any water molecules that are directly solvating a solute molecule are then identified and excluded from further analysis. This is defined by a cut off distance corresponding to the first minima in the  $O_wX$  RDF where X is the solute atom/molecule. This step is included as strong interactions between water molecules and solute molecules can allow the hydration water molecules to adopt energetically unfavourable conformations relative to other, neighbouring, water molecules. Therefore, when water molecules of this nature are included in the hydrogen bond analysis there will be a tendency for the average interaction energy between two hydrogen bonded water molecules to be overestimated, and hence the network will appear to be less enthalpically stable. This also helps to minimise any effects the heterogeneity between local water environments that are present in aqueous solutions would have on the measured geometric and energetic distributions. This is because the geometry of neighbouring water molecules in the hydration shell of solute molecules will certainly be different than in the bulk. By considering only the bulk water molecules, and disregarding any hydration water, the effects of the solute on the bond network are more reliably observed. This feature was not present in the original routine<sup>57</sup>.

A topological definition of hydrogen bonding is used, broadly similar to the approach used in previous literature<sup>63-65</sup>, where a water molecule is deemed to be hydrogen bonded to a central molecule if it simultaneously satisfies two criteria: the water molecule's oxygen must be within a distance to the central molecule's oxygen corresponding to the first minima in the  $O_wO_w$  RDF, and the water molecule's hydrogen must be within a distance to the central molecule's oxygen corresponding to the first minima in the  $O_wH_w$  RDF. This allows for increased flexibility in defining a hydrogen bond, as strict geometric or energetic criterias<sup>65-72</sup> would be inadequate to describe a system that is perturbed by the addition of solute molecules. Based on this definition the hydrogen bond donor and acceptor angles, total interaction energies between hydrogen bonded molecules, as well as the abundance of specific hydrogen bonding conformations such as bifurcated oxygens and cyclic dimers are calculated.

## 4. Results

### a. NMR study of hydrogen bonding in TMAO : $Mg(ClO_4)_2$ aqueous solutions

To examine hydrogen bonding in the tertiary aqueous solution, NMR experiments measured the relative position of the  $^1H$  NMR water peak as a function of solute concentration. All NMR experiments were completed over a concentration range of 0 – 1.0 mol/kg  $H_2O$  in increments of 0.2 mol/kg  $H_2O$  for both solutes at 27°C, as outlined in section 3(a), resulting in 36 samples. As outlined in section 3(b), a stronger hydrogen bond results in increased deshielding of the hydrogen nucleus and a shift downfield (higher ppm) of the associated NMR peak. The shift of the NMR peak from the water hydrogen data is presented in figure 1 below. These results show a downfield shift upon addition of TMAO, suggesting strengthened hydrogen bonding between water molecules. An upfield shift upon  $Mg(ClO_4)_2$  addition is observed, suggesting weakened hydrogen bonding between water molecules. The perturbation to water structure is therefore opposite for each solute, and act to cancel each other out when in combination. This supports previous neutron diffraction experiments<sup>57</sup>, which showed that TMAO restores the hydrogen bonding network of water when perturbed by  $Mg(ClO_4)_2$ .

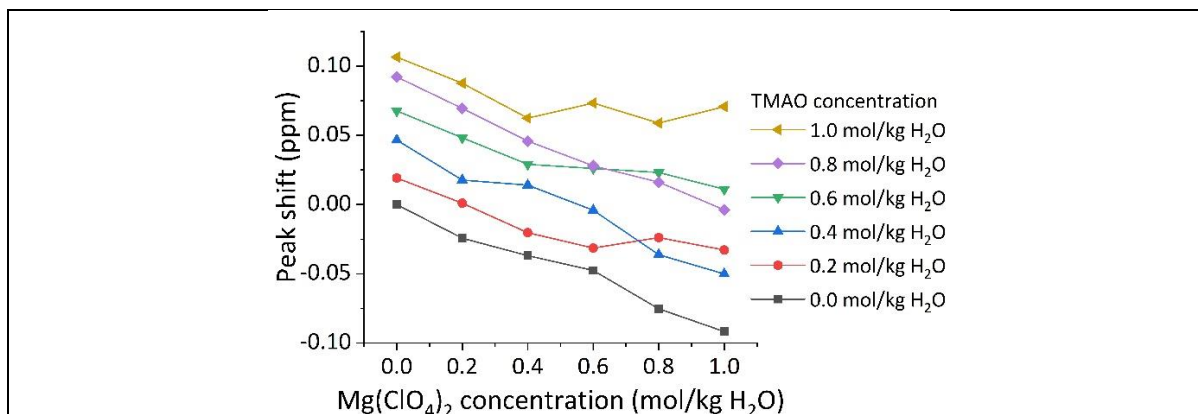


**Figure 1.** <sup>1</sup>H NMR peak shift data for mixed aqueous Mg(ClO<sub>4</sub>)<sub>2</sub> and TMAO from 0 – 1.0 mol/kg H<sub>2</sub>O in increments of 0.2 mol/kg H<sub>2</sub>O relative to the value for pure water. Data shows that Mg(ClO<sub>4</sub>)<sub>2</sub> results in negative peak shifts, corresponding to weaker hydrogen bonding, and TMAO results in positive peak shifts, corresponding to strengthened hydrogen bonding. The two solutes appear to act in opposition to one another.

b. NMR study of dynamics of water molecules in TMAO : Mg(ClO<sub>4</sub>)<sub>2</sub> aqueous solutions

The inverse  $T_1$  decay time and diffusion coefficient for water molecule hydrogens present in the system as a function of Mg(ClO<sub>4</sub>)<sub>2</sub> and TMAO concentration at 27°C are presented in figure 2. These results for pure water,  $D \approx 2.3 \times 10^{-9} \text{m}^2 \text{s}^{-1}$  and  $T_1 \approx 3.0 \text{s}$ , are consistent with previously reported values<sup>73,74</sup>. As shown in figures 2(a) and 2(b) both solutes slow the dynamics of the water molecules present in the system. This is indicated by the increasing relaxation rate  $T_1^{-1}$ , and therefore increasing rotational correlation time with increasing solute concentration, and by a decreasing diffusion coefficient as a function of increasing solute concentration. This is unsurprising<sup>75</sup> as both TMAO and Mg<sup>2+</sup> interact more strongly with water molecules than water molecules interact with themselves, as shown in our previous work<sup>57</sup>. Previous literature have shown that the interactions between water molecules and ClO<sub>4</sub><sup>-</sup> are weaker than between neighbouring water molecules in pure water and are therefore expected to exhibit increased dynamics<sup>75-77</sup>, however our results clearly demonstrate that these effects, if present, are overpowered by the strong interactions between water molecules and Mg<sup>2+</sup>/TMAO. Our results also show that any dynamic heterogeneities in the aqueous solution due to perturbed dynamics of water molecules in the first hydration shell of the solutes are minimal. This is clearly demonstrated by the data used to determine the  $T_1$  times for the samples as described in section 3(b) (example data shown in Fig S2). The  $T_1$  times are determined by fitting these data to the expression shown in equation 1. Any dynamic heterogeneities would result in multiple  $T_1$  decay times and therefore the data would need to be described by multiple exponential terms. As the data is clearly extremely well described using a single exponential, this indicates that any dynamic heterogeneities across all samples are minimal. Both Mg(ClO<sub>4</sub>)<sub>2</sub> and TMAO therefore act to slow water dynamics and this perturbation is additive.

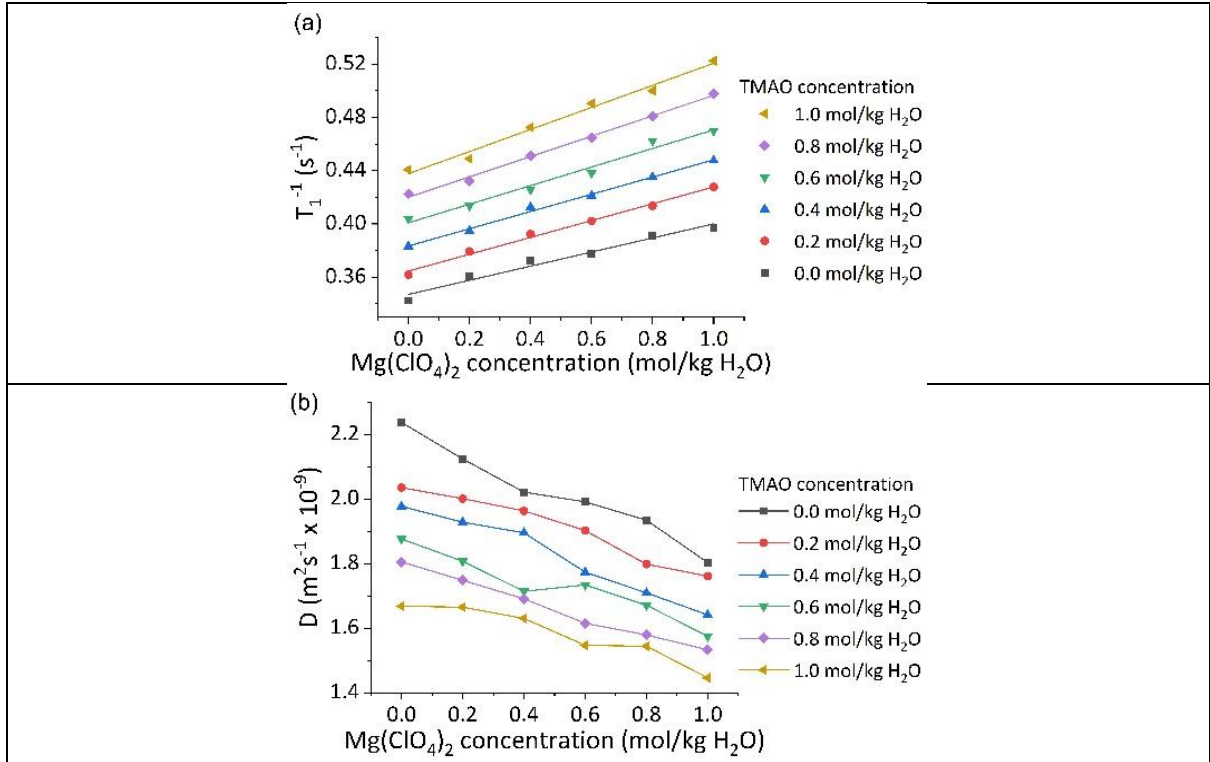


**Figure 2.** (a) Inverse  $T_1$  decay time (proportional to rotational correlation time) from NMR experiments as a function of solute concentration (b) Diffusion coefficient of water molecules as a function of solute concentration. An increasing rotational correlation time and decreasing diffusion coefficient with increasing solute concentration is indicative of slowed water molecule dynamics. The two solutes appear to act additively.

The diffusion coefficient  $D$  is inversely proportional to the viscosity  $\eta$  experienced by the the water molecule, as shown by the Stokes-Einstein relation (equation 3), where  $T$  is temperature,  $k_B$  is Boltzmann's constant, and  $r_h$  is the hydrodynamic radius of the molecule<sup>78</sup>.

$$D = \frac{k_B T}{6\pi\eta r_h} \quad (3)$$

A similar expression can be derived that considers rotational diffusion, rather than translational diffusion, known as the Debye-Einstein relationship (equation 4). This shows that the rotational correlation time  $\tau_{RTC}$  is proportional to the local viscosity.

$$T_1^{-1} \propto \tau_{RTC} = \frac{4\pi\eta r_h^3}{3k_B T} \quad (4)$$

It therefore follows that if translational diffusion and rotational diffusion are governed by the same local viscosity<sup>79</sup>, that  $D \propto \tau_{RTC}^{-1} \propto T_1$ . We therefore plot the spin lattice relaxation rate against the diffusion coefficient for each sample in figure 3. This shows a linear dependence and indicates that translational diffusion and rotational diffusion are indeed governed by the same local microscale viscosity. This also supports the assumption that the spin lattice relaxation rate  $T_1$  is dominated by rotational motion.

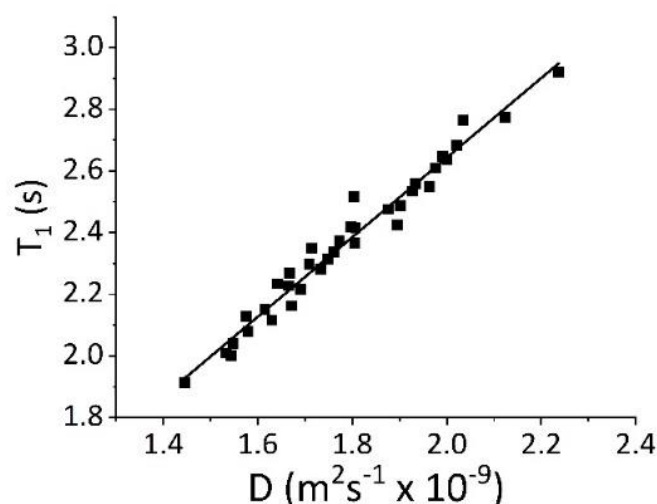


**Figure 3.** Spin-lattice relaxation rate ( $T_1$ ) decay time as a function of diffusion coefficient  $D$  for mixed  $\text{Mg}(\text{ClO}_4)_2$  and TMAO tertiary aqueous solutions from 0 – 1.0 mol/kg  $\text{H}_2\text{O}$  in increments of 0.2 mol/kg  $\text{H}_2\text{O}$  for each solute. Linear relationship between both properties for each sample shows water molecules experience the same local viscosity for both translational diffusion and rotational motion.

### c. Neutron diffraction data and computational modelling

Neutron diffraction data and computational modelling allow for an examination of the structure the hydrogen bonding in the tertiary aqueous solution, as described in section 3(g), as well as the local structures present in the aqueous solution through RDFs, coordination numbers, spatial density functions, etc. A complete description of perturbations to water structure in aqueous  $\text{Mg}(\text{ClO}_4)_2$  and TMAO using these methods can be found in our recent publication<sup>57</sup> and will not be further discussed here. Details of the solute-solute coordination numbers can be found in the supporting information (Table S3). This data shows that solute-solute interactions between  $\text{Mg}^{2+}$  and  $\text{ClO}_4^-$  ions are minimal as evidenced by coordination numbers substantially below 1, even at the highest concentration of 2.7 M. The solute-solute interactions between TMAO molecules are shown to be moderate, consistent with neutron scattering data by Meersman et al<sup>28</sup>. and are most likely driven by hydrophobic association. However, in the presence of 2.7 M  $\text{Mg}(\text{ClO}_4)_2$  this interaction is substantially reduced and replaced by favourable interactions between  $\text{ClO}_4^-$  ions. Due to the weak interactions between  $\text{ClO}_4^-$  ions and water molecules<sup>75–77</sup> this interaction is also likely hydrophobically driven.

Figure 4 shows the average hydrogen bond interaction energy between two water molecules for binary and tertiary solutions containing TMAO and  $\text{Mg}(\text{ClO}_4)_2$  and pure water, and show excellent agreement with previous literature<sup>69</sup>. An increase in the average hydrogen bond interaction energy upon addition of each solute is measured relative to pure water, suggesting a reduction in the stability of the average hydrogen bond between two water molecules. This is likely due to an excluded volume effect of the solute. However, for samples containing both 1.0 M TMAO and  $\text{Mg}(\text{ClO}_4)_2$  at concentrations of 0.2 M and 2.7 M the average hydrogen bond interaction energy decreases towards the value measured for pure water. This suggests that while individually both solutes act to reduce the stability of water molecule hydrogen bonding, when together this perturbation is absent, and the two solutes cancel each other out. The full conformational energy density maps, such as those reported in the previous work, are available in the supporting information (Fig S4).

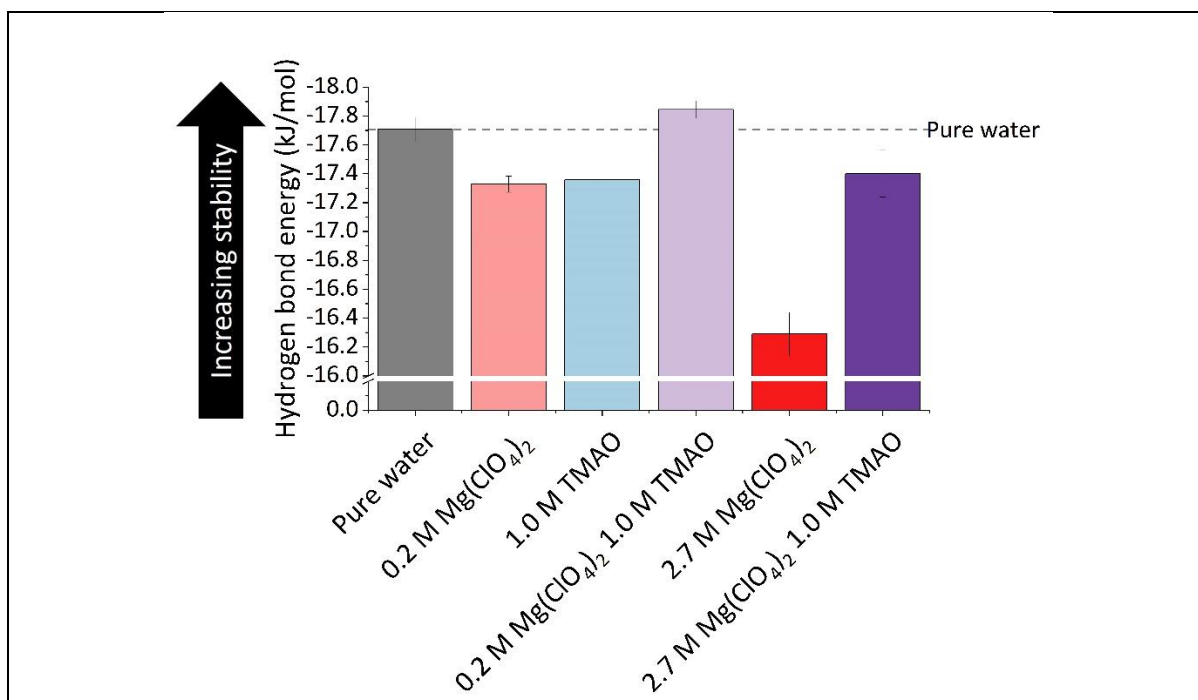


**Figure 4.** Average hydrogen bond interaction energy ( $E$ ) for pairs of hydrogen bonded water molecules in the bulk for all samples calculated as previously described in section 3(g)<sup>57</sup>. The inclusion of either  $\text{Mg}(\text{ClO}_4)_2$  or TMAO individually results in less stable hydrogen bonds. The inclusion of both solute species simultaneously results in more stable hydrogen bonds, more reminiscent of those found in pure water.

d. Extended hydrogen bonding analysis: Examination of hydrogen bonded conformations

Using neutron diffraction data and computational modelling we examine the hydrogen bonded conformations in the tertiary solution. The conformations the current routine is capable of identifying include cyclic dimers, bifurcated oxygens, hydrogen bonded pairs of molecules with a positive overall interaction energy, and bifurcated hydrogens. Their relative abundance in binary and tertiary solutions of TMAO and  $\text{Mg}(\text{ClO}_4)_2$  were found (Fig S5). Bifurcated hydrogen conformations are an intermediate step that occurs as a water molecule switches hydrogen bonding partners. During this switching event a water molecule simultaneously donates a hydrogen bond to two neighbouring water molecules through a single hydrogen as illustrated in figure 5(a). The relative abundance of water molecules in a bifurcated hydrogen conformation in water decreases with increasing solute concentration (Fig 5(b)). Such a reduction in bifurcated hydrogen conformations is consistent with less frequent hydrogen bond switching events, and hence slower dynamics, as observed for the increased inverse  $T_1$  decay time and decreased diffusion coefficient with increasing solute concentration (Fig 2).

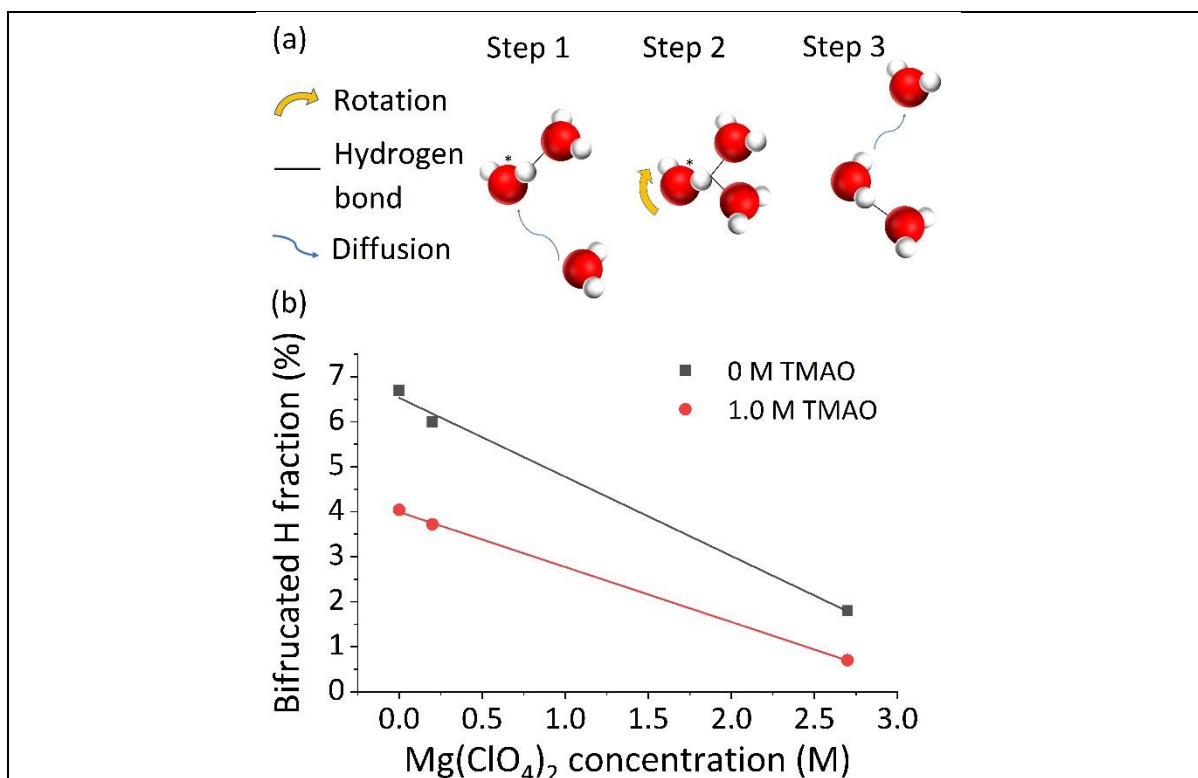


**Figure 5.** (a) The bifurcated hydrogen conformation occurs as an intermediate as a water molecule switches hydrogen bonding partners. (b) Fraction of water molecules with a bifurcated hydrogen bond for each sample studied by neutron diffraction. A decreasing fraction of bifurcated hydrogen conformations with increasing solute concentration is therefore consistent with reduced dynamics. Error bars are negligible.

e. Quantifying TMAO relative to Mg(ClO<sub>4</sub>)<sub>2</sub>

At this point it should be clear that if one considers the effect of the two solutes on the structure of bulk water then they act in opposition to one another, with one solute effectively cancelling out the other, whereas if one considers the effect of the two solutes on the dynamics of water they act additively, where the inclusion of one solute results in reduced dynamics and the inclusion of the second slows dynamics yet further. We will now attempt to quantify the ability of one solute as a perturbing agent relative to the other. This can be achieved by plotting all the data as a function of the effective total concentration such that all points for a given dataset lie on a single master curve. The effective total concentration is described in equation 5 below where  $[x]$  is the concentration of  $x$  in mol/kg H<sub>2</sub>O and  $g$  is a dimensionless weighting factor that represents how effective TMAO is as a perturbing agent relative to Mg(ClO<sub>4</sub>)<sub>2</sub>. A straight line is then fit to the resultant master curve data. The quality of the linear fit to the data is quantified by the calculated  $r^2$  value, which gives a score from 0-1. The  $r^2$  value is then monitored as a function of  $g$  to determine the optimum  $g$  value. It is important to note here that when using this method, we are concerned solely with the quality of the linear fit, and not the gradient or intercept of the fit itself.

$$[Eff] = [Mg(ClO_4)_2] + g[TMAO] \quad (5)$$

Five datasets were chosen for this method of analysis: the peak shift NMR data (Fig 1), the inverse T<sub>1</sub> NMR data (Fig 2(a)), the diffusion coefficient data (Fig 2(b)), the bulk average hydrogen bond interaction energy predicted by neutron diffraction and EPSR (Fig 4), and the fraction of bulk water molecules with a bifurcated hydrogen predicted by neutron diffraction and EPSR (Fig 5). These datasets

were chosen as they represent both dynamic and structural measures of the system. The peak shift NMR data and bulk average hydrogen bond interaction energy represent perturbations to structural hydrogen bonding as a result of the two solutes. The inverse  $T_1$  data and diffusion coefficient data represent dynamic measures of the system that are measured through well-established means<sup>36-38</sup>. The fraction of bulk water molecules with a bifurcated hydrogen corresponds to the intermediate step in the bond switching mechanism outlined by the extended jump model proposed by Laage and Hynes<sup>47,80</sup>. It is important to note that the data is plotted using the absolute value of the weighting parameter. This is because the two solutes act to oppose one another from a structural perspective, and therefore have a negative weighting parameter, whereas they act additively from a dynamic perspective, and therefore have a positive weighting parameter. Plotting the absolute value makes the data sets more directly comparable. The results are shown in figure 6.

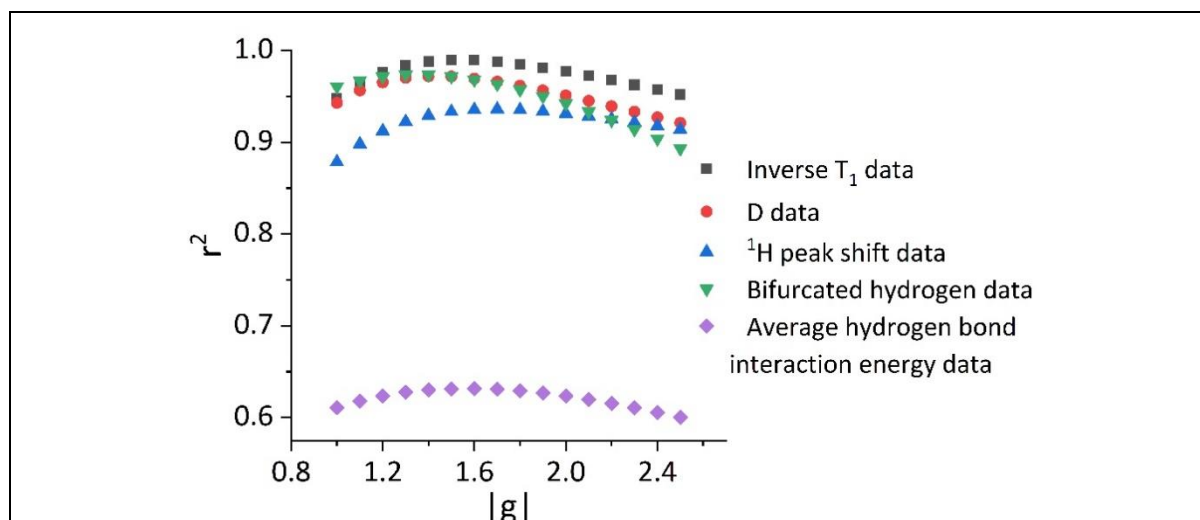


**Figure 6.** Combining each dataset as a function of effective total solute concentration  $[Eff] = [Mg(ClO_4)_2] + g[TMAO]$  for inverse  $T_1$  decay time data, diffusion coefficient data,  $^1H$  NMR peak shift data, relative abundance of bifurcated hydrogens, and average interaction energy between two hydrogen bonded molecules.  $[x]$  is the concentration of solute  $x$  in mol/kg  $H_2O$  and  $g$  is a weighting parameter. The resultant master curves are fit using a linear expression. The quality of the fit, which is scored between 0 for poor quality linear fits and 1 for high quality linear fits as determined by its  $r^2$  is plotted as a function of the absolute weighting parameter  $g$ . The location of the peak of the resultant curves shown above corresponds to the optimum value of  $g$ . This  $g$  value therefore quantifies the ability of  $Mg(ClO_4)_2$  to perturb water structure and dynamics relative to TMAO.

A high-quality linear fit can be achieved to the inverse  $T_1$  (Fig 7(a)), diffusion coefficient (Fig S7(a)), peak shift (Fig S7(b)), and bifurcated hydrogen data (Fig 7(b)), as shown by a maximum  $r^2$  value approaching unity and shown in figure 6. However, a linear fit to the average hydrogen bond interaction energy data is of much lower quality and may result from the assumptions that go into producing this data (Fig S7(c)). This is related to the difficulty accurately describing a hydrogen bond between water molecules, to which there is still no definitively accepted answer<sup>65,67</sup>. This could also be a result of the intrinsic limitations of neutron diffraction and EPSR, as neutron diffraction data requires correction for multiple scattering, attenuation and inelasticity effects<sup>12</sup> before EPSR can be performed, and EPSR does not guarantee a unique solution, merely one that is consistent with the corrected scattering data. The peak in each of these 5 data sets represents the optimum weighting parameter. This was determined by numerically differentiating the datasets (Fig S6). These results, along with the averaged value and its standard uncertainty are given in table 1. This shows an overall consistency of the optimum  $g$  value taken from 5 different sources across 2 different experimental techniques and 3 different experimental apparatus, and when considering both dynamic and structural perturbations to the system. Within the dynamic measures of the system it also shows a consistency across multiple length scales. Using the

diffusion coefficient data presented in figure 2 and the experimental diffusion time of 60 ms, a water molecule has a root-mean-square deviation of 20-30 microns in this time period, corresponding to approximately 83,000 water molecule diameters.

Data set	Absolute $g$ value
Inverse $T_1$	1.563
Diffusion coefficient	1.442
Peak shift NMR	1.727
Bifurcated hydrogen	1.370
Averaged hydrogen bond interaction energy	1.579
Average value	$1.54 \pm 0.06$

**Table 1.** Optimum weighting parameter calculated by the peak location of quality of linear fit for each data set ( $r^2$ ) as a function of weighting parameter ( $g$ ) for each of the 5 data sets. The optimum weight parameter corresponds to the highest quality linear fit of the data plotted using effective total concentration.

TMAO can therefore be thought of as being a factor of  $1.54 \pm 0.06$  more “effective” at perturbing water structure and dynamics than  $\text{Mg}(\text{ClO}_4)_2$ . The inverse  $T_1$  data and bifurcated hydrogen data using the effective total concentration at this average optimum  $g$  value are plotted in figure 7. The remaining data sets are shown in the supporting information (Fig S7), and example inverse  $T_1$  data using the extreme  $g$  values of 0.9 and 2.4 are shown in Fig S8.

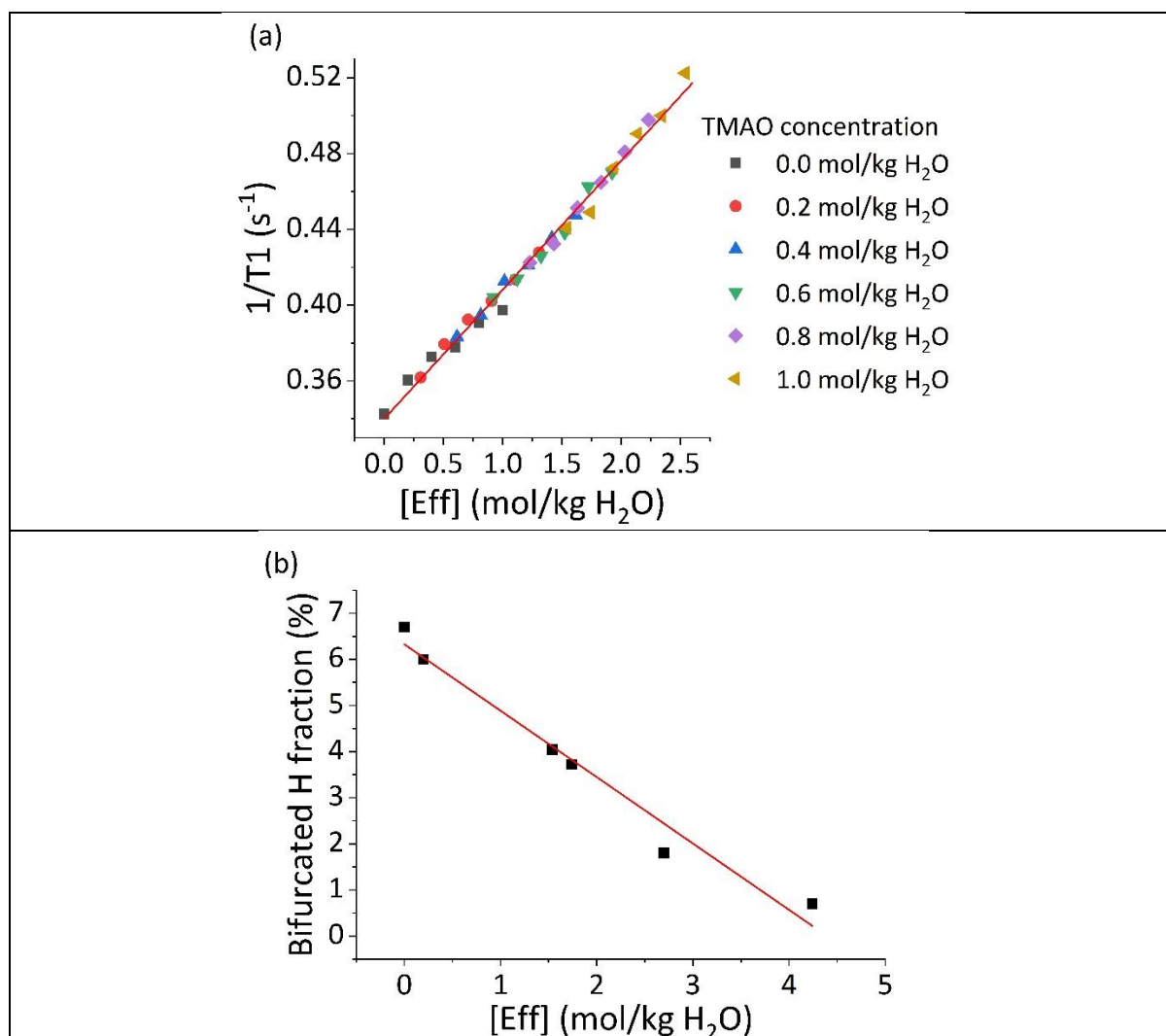


**Figure 7.** Replotting data sets using effective total concentration described by  $[Eff] = [Mg(ClO_4)_2] + g[TMAO]$  where  $[x]$  is the concentration of solute  $x$  in mol/kg H<sub>2</sub>O and  $g$  is a weighting factor. Weighting factor is set to 1.54, the average optimum weighting factor as described in figure 6. (a) Inverse  $T_1$  data, (b) Bifurcated hydrogen data. Remaining datasets can be found in supporting information (Fig S7). Error bars are negligible.

## 5. Discussion

This study of TMAO and  $Mg(ClO_4)_2$  reveals the surprising result that while the two solutes perturb water structure in an opposing manner with one solute cancelling out the other, they act to perturb water dynamics in an additive manner, both acting to slow water dynamics.

The identification of the fraction of bulk water molecules with a bifurcated hydrogen, inspired by the so called “extended jump model” of Laage and Hynes<sup>47,54,75,80–82</sup>, suggests dynamic changes in the system, and allows the extended jump model to be applied to neutron diffraction data for the first time. The model proposes that water dynamics is the sum of two parts; (i) a large angular jump through a bifurcated hydrogen intermediate as a water molecule switches hydrogen bonding partners from an over-coordinated first shell neighbour to an under-coordinated second shell neighbour, and (ii) diffusion of water molecules that maintain a hydrogen bond called frame reorientation. Measuring the relative abundance of bifurcated hydrogens, as demonstrated here, could serve as an indication for modifications to system dynamics, provided that the jump reorientation is the dominant mechanism for the water dynamics in the system of interest. This can then be validated by NMR, as has been done in this work. It is important to note here that the analysis of the inverse  $T_1$  employed in this work and described in equation 4 assumes diffusive rotational motion of water molecules, which is in contradiction to the large angular jumps described by the extended jump model. We rationalise this disparity by considering the difference in scale between these two datasets. The abundance of bifurcated hydrogens calculated through computer simulations based on neutron scattering data considers each water molecule individually, whereas the inverse  $T_1$  measurements from NMR data considers an ensemble average over the whole sample. When considering the whole sample in this way, the ensemble average of many large angular jumps would appear to be rotational diffusion, in the same way that the ensemble average of many particles undergoing Brownian motion would appear to be translational diffusion. However, when employing the extended jump model as we have done in this work, it is crucially important to consider two factors: the excluded volume effect of the solute, and the frame reorientation mechanism.

The inclusion of a solute molecule into water creates an excluded volume in the water network due to the physical space the solute molecule occupies. This occupation of space makes it less probable that water molecules will be appropriately placed to adopt the bifurcated hydrogen bonded conformation. One would therefore expect the fraction of hydrogen bonded water molecules with a bifurcated hydrogen to decrease with increasing solute concentration for a purely hydrophobic solute. If this is an indication of dynamic information it could mistakenly be concluded that the solute is slowing the dynamics of water molecules, when this may not necessarily be the case. In order to ensure the results from this research are not a result of this effect we can consider the TMAO- $O_w$ ,  $Mg^{2+}$ - $O_w$  and  $ClO_4^-O_w$   $g(r)$ s (Fig S9). By considering the location of the first peak in this RDF, we can estimate the effective volume the solute molecule occupies. Modelling the TMAO molecule as a sphere with its nitrogen atom at its centre, the total volume occupied by its hydration sphere is approximately 387 Å<sup>3</sup>. Similarly for the  $ClO_4^-$  ion, treating it as a sphere with its chlorine atom at its centre, its hydration sphere is approximately 256 Å<sup>3</sup>.  $Mg^{2+}$  in turn has a hydration sphere of approximately 18 Å<sup>3</sup>. Assuming complete dissolution of the two ions with no hydration shell overlap, the total volume in solution occupied by a single  $Mg(ClO_4)_2$  molecule is approximately 530 Å<sup>3</sup>. If the observed results were solely as a result of the excluded volume effects one would therefore expect a weighting parameter equivalent to the ratio of the TMAO exclude volume to the total  $Mg(ClO_4)_2$  excluded volume, which is approximately 0.73 (see Derivation S1 in SI). . As this is not the case, and the weighting parameter derived from EPSR data

is consistent with that derived from NMR data, this suggests that using the bifurcated hydrogen bond fraction as an indication of dynamic information is a suitable technique for this system. For this tertiary system we have also shown that rotational dynamics and diffusion are both dependent on the same local viscosity (Fig 3), allowing for meaningful comparison between the criteria used to compare dynamic perturbations used here.

The consideration of the frame reorientation component of the extended jump model<sup>47,80,81</sup> is not available from EPSR. EPSR is a Monte Carlo based technique, and hence molecular reorientations are performed randomly, and their success is based on their stability in their new location and orientation. These systems would have to be investigated more thoroughly using a combination of various techniques such as Molecular Dynamics, NMR, IR-spectroscopy, and bulk viscosity measurements.

A final important implication of this work relates to the hydrophobic effect. A classical view of this effect is that the introduction of a hydrophobic solute results in a rigid cage of highly structured water molecules solvating the solute, and an associated entropy penalty<sup>9,83</sup>. Bringing the two solutes together requires fewer water molecules to solvate the solutes, and therefore a lower entropy penalty. However, there has been little direct evidence for highly structured water around hydrophobic solutes, so the origins of the hydrophobic effect may not be a result of enhanced structure, but perturbed dynamics near the solute. It is therefore important to consider both aspects simultaneously, such as has been done in this work.

## 6. Conclusion

In this work the competing effects in a tertiary aqueous system between TMAO and  $\text{Mg}(\text{ClO}_4)_2$  on water structure and dynamics have been quantified using NMR and neutron scattering with subsequent EPSR. This shows that while the two solutes perturb water structure in an opposing manner, they perturb water dynamics in an additive manner in the concentration ranges studied here. By plotting the data as a function of total solute concentration with an additional weighting parameter we have been able to quantify these effects, and have shown that TMAO is a more effective perturbing agent by a factor of  $1.54 \pm 0.06$  than  $\text{Mg}(\text{ClO}_4)_2$ . We believe this relatively simple technique could be easily applied to any complex aqueous systems.

The fact that opposite results are drawn from dynamics and structure shows that one cannot draw simple assumptions from a single technique, and that any assumptions made from one set of data must be tested using an appropriate alternative technique. While NMR has been used to help guide EPSR studies on peptides, for example by helping to identify the ratio of cis to trans isomers in polypeptides<sup>20,30,84</sup>, a true correlative study on a single system such as this one is yet to be reported.

## 7. Supporting Information

The supporting information document accompanying this publication contains: a complete list of samples studied by neutron diffraction, the parameters of the EPSR simulations including Lennard-Jones and Coulomb parameters for each atomic species present and the size of the simulations, example NMR data of aqueous potassium halides, example data for the calculation of the spin-lattice relaxation rate  $T_1$ , a summary of the solute-solute coordination numbers determined by EPSR, example EPSR fits to the scattering data, the conformational energy density plots for each sample determined through the hydrogen bond analysis routine, the abundance of specific hydrogen bonded conformations determined through the hydrogen bond analysis routine, the numerically differentiated data presented in Fig 6 used to determine the peak location, the remaining 3 datasets described in Fig 7 plotted using the effective total concentration, and the inverse  $T_1$  dataset plotted as a function of effective total solute concentration using a weighting parameter of 0.9 and 2.4.

## 8. Acknowledgements

The project was supported by a grant from the Engineering and Physical Sciences Research Council (EPSRC) (EP/P02288X/1) to Prof. L. Dougan. H. Laurent is supported by an ISIS Facility Development and Utilisation Studentship and an EPSRC DTA studentship. We are grateful to the STFC and ISIS neutron and muon facility for beamtime on NIMROD (RB1910455) and support from Drs Tom Headen and Tristan Youngs. We thank all members of the Dougan group for their support and feedback.

## 9. References

- (1) Ball, P. Water Is an Active Matrix of Life for Cell and Molecular Biology. *Proc. Natl. Acad. Sci.* **2017**, *114* (51), 13327–13335. <https://doi.org/10.1073/pnas.1703781114>.
- (2) Bellissent-Funel, M. C.; Hassanali, A.; Havenith, M.; Henschman, R.; Pohl, P.; Sterpone, F.; Van Der Spoel, D.; Xu, Y.; Garcia, A. E. Water Determines the Structure and Dynamics of Proteins. *Chem. Rev.* **2016**, *116* (13), 7673–7697. <https://doi.org/10.1021/acs.chemrev.5b00664>.
- (3) Soper, A. K. The Radial Distribution Functions of Water as Derived from Radiation Total Scattering Experiments: Is There Anything We Can Say for Sure? *ISRN Phys. Chem.* **2013**, *2013*, 1–67. <https://doi.org/10.1155/2013/279463>.
- (4) Szent-Györgyi, A. Biology and Pathology of Water. *Perspect. Biol. Med.* **1971**, *14* (2), 239–249. <https://doi.org/10.1353/pbm.1971.0014>.
- (5) Amann-Winkel, K.; Bellissent-Funel, M. C.; Bove, L. E.; Loerting, T.; Nilsson, A.; Paciaroni, A.; Schlesinger, D.; Skinner, L. X-Ray and Neutron Scattering of Water. *Chem. Rev.* **2016**, *116* (13), 7570–7589. <https://doi.org/10.1021/acs.chemrev.5b00663>.
- (6) Zhao, L.; Ma, K.; Yang, Z. Changes of Water Hydrogen Bond Network with Different Externalities. *Int. J. Mol. Sci.* **2015**, *16* (4), 8454–8489. <https://doi.org/10.3390/ijms16048454>.
- (7) Marcus, Y. Effect of Ions on the Structure of Water: Structure Making and Breaking. *Chemical Reviews*. 2009, pp 1346–1370. <https://doi.org/10.1021/cr8003828>.
- (8) Gallo, P.; Amann-Winkel, K.; Angell, C. A.; Anisimov, M. A.; Caupin, F.; Chakravarty, C.; Lascaris, E.; Loerting, T.; Panagiotopoulos, A. Z.; Russo, J. et al. Water: A Tale of Two Liquids. *Chem. Rev.* **2016**, *116* (13), 7463–7500. <https://doi.org/10.1021/acs.chemrev.5b00750>.
- (9) Ball, P. *H<sub>2</sub>O A Biography of Water*, First.; Weidenfeld and Nicolson: London, 2000.
- (10) Brini, E.; Fennell, C. J.; Fernandez-Serra, M.; Hribar-Lee, B.; Lukšič, M.; Dill, K. A. How Water's Properties Are Encoded in Its Molecular Structure and Energies. *Chem. Rev.* **2017**, *117* (19), 12385–12414. <https://doi.org/10.1021/acs.chemrev.7b00259>.
- (11) Dill, K. A.; Truskett, T. M.; Vlachy, V.; Hribar-lee, B. Modeling Water, the Hydrophobic Effect. *Annu. Rev. Biophys. Biomol. Struct.* **2005**, *34*, 173–199. <https://doi.org/10.1146/annurev.biophys.34.0402>.
- (12) Soper, A. K. *Rutherford Appleton Laboratory Technical Report RAL-TR-2011-013*; 2011; Vol. RAL-TR-201.
- (13) Lenton, S.; Rhys, N. H.; Towey, J. J.; Soper, A. K.; Dougan, L. Highly Compressed Water Structure Observed in a Perchlorate Aqueous Solution. *Nat. Commun.* **2017**, *8* (1), 1–5. <https://doi.org/10.1038/s41467-017-01039-9>.
- (14) Mancinelli, R.; Botti, A.; Bruni, F.; Ricci, M. A.; Soper, A. K. Hydration of Sodium, Potassium, and Chloride Ions in Solution and the Concept of Structure Maker/Breaker. *J. Phys. Chem. B* **2007**, *111* (48), 13570–13577. <https://doi.org/10.1021/jp075913v>.
- (15) Soper, A. K.; Weckström, K. Ion Solvation and Water Structure in Potassium Halide Aqueous

- Solutions. *Biophys. Chem.* **2006**, *124* (3), 180–191. <https://doi.org/10.1016/j.bpc.2006.04.009>.
- (16) Mancinelli, R.; Botti, A.; Bruni, F.; Ricci, M. A.; Soper, A. K. Perturbation of Water Structure Due to Monovalent Ions in Solution. *Phys. Chem. Chem. Phys.* **2007**, *9* (23), 2959–2967. <https://doi.org/10.1039/b701855j>.
- (17) Busch, S.; Lorenz, C. D.; Taylor, J.; Pardo, L. C.; McLain, S. E. Short-Range Interactions of Concentrated Proline in Aqueous Solution. *J. Phys. Chem. B* **2014**, *118*, 14267–14277. <https://doi.org/10.1021/jp508779d>.
- (18) Rhys, N. H.; Soper, A. K.; Dougan, L. The Hydrogen-Bonding Ability of the Amino Acid Glutamine Revealed by Neutron Diffraction Experiments. *J. Phys. Chem. B* **2012**, *116* (45), 13308–13319. <https://doi.org/10.1021/jp307442f>.
- (19) McLain, S. E.; Soper, A. K.; Watts, A. Water Structure around Dipeptides in Aqueous Solutions. *Eur. Biophys. J.* **2008**, *37* (5), 647–655. <https://doi.org/10.1007/s00249-008-0292-1>.
- (20) Busch, S.; Bruce, C. D.; Redfield, C.; Lorenz, C. D.; McLain, S. E. Water Mediation Is Essential to Nucleation of Beta-Turn Formation in Peptide Folding Motifs. *Angew. Chemie - Int. Ed.* **2013**, *52* (49), 13091–13095. <https://doi.org/10.1002/anie.201307657>.
- (21) Daidone, I.; Iacobucci, C.; McLain, S. E.; Smith, J. C. Alteration of Water Structure by Peptide Clusters Revealed by Neutron Scattering in the Small-Angle Region (below  $1 \text{ \AA}^{-1}$ ). *Biophys. J.* **2012**, *103* (7), 1518–1524. <https://doi.org/10.1016/j.bpj.2012.08.010>.
- (22) McLain, S. E.; Soper, A. K.; Daidone, I.; Smith, J. C.; Watts, A. Charge-Based Interactions between Peptides Observed as the Dominant Force for Association in Aqueous Solution. *Angew. Chemie - Int. Ed.* **2008**, *47* (47), 9059–9062. <https://doi.org/10.1002/anie.200802679>.
- (23) Scoppola, E.; Sodo, A.; McLain, S. E.; Ricci, M. A.; Bruni, F. Water-Peptide Site-Specific Interactions: A Structural Study on the Hydration of Glutathione. *Biophys. J.* **2014**, *106* (8), 1701–1709. <https://doi.org/10.1016/j.bpj.2014.01.046>.
- (24) Rhys, N. H.; Soper, A. K.; Dougan, L. Hydrophilic Association in a Dilute Glutamine Solution Persists Independent of Increasing Temperature. *J. Phys. Chem. B* **2015**, *119* (51), 15644–15651. <https://doi.org/10.1021/acs.jpcc.5b07413>.
- (25) Soper, A. K.; Edler, K. J. Coarse-Grained Empirical Potential Structure Refinement: Application to a Reverse Aqueous Micelle. *Biochim. Biophys. Acta - Gen. Subj.* **2017**, *1861* (6), 1652–1660. <https://doi.org/10.1016/j.bbagen.2017.02.028>.
- (26) Laurent, H.; Soper, A.; Dougan, L. Biomolecular Self-Assembly under Extreme Martian Mimetic Conditions. *Mol. Phys.* **2019**, *117* (22), 3398–3407. <https://doi.org/10.1080/00268976.2019.1649485>.
- (27) Soper, A. K.; Castner, E. W.; Luzar, A. Impact of Urea on Water Structure: A Clue to Its Properties as a Denaturant? *Biophys. Chem.* **2003**, *105* (2–3), 649–666. [https://doi.org/10.1016/S0301-4622\(03\)00095-4](https://doi.org/10.1016/S0301-4622(03)00095-4).
- (28) Meersman, F.; Bowron, D.; Soper, A. K.; Koch, M. H. J. Counteraction of Urea by Trimethylamine N-Oxide Is Due to Direct Interaction. *Biophys. J.* **2009**, *97* (9), 2559–2566. <https://doi.org/10.1016/j.bpj.2009.08.017>.
- (29) Meersman, F.; Bowron, D.; Soper, A. K.; Koch, M. H. J. An X-Ray and Neutron Scattering Study of the Equilibrium between Trimethylamine N-Oxide and Urea in Aqueous Solution. *Phys. Chem. Chem. Phys.* **2011**, *13* (30), 13765–13771. <https://doi.org/10.1039/c1cp20842j>.
- (30) Steinke, N.; Genina, A.; Lorenz, C. D.; McLain, S. E. Salt Interactions in Solution Prevent Direct Association of Urea with a Peptide Backbone. *J. Phys. Chem. B* **2017**, *121* (8), 1866–1876. <https://doi.org/10.1021/acs.jpcc.6b12542>.

- (31) Lenton, S.; Rhys, N. H.; Towey, J. J.; Soper, A. K.; Dougan, L. Temperature Dependent Segregation in Alcohol-Water Binary Mixtures Is Driven by Water Clustering. *Journal of Physical Chemistry B*. 2018, pp 7884–7894. <https://doi.org/10.1021/acs.jpcc.8b03543>.
- (32) Dougan, L.; Hargreaves, R.; Bates, S. P.; Finney, J. L.; Rat, V.; Soper, A. K.; Crain, J. Segregation in Aqueous Methanol Enhanced by Cooling and Compression. *J. Chem. Phys.* **2005**, *122* (17), 174517. <https://doi.org/10.1063/1.1888405>.
- (33) Soper, A. K.; Dougan, L.; Crain, J.; Finney, J. L. Excess Entropy in Alcohol-Water Solutions: A Simple Clustering Explanation. *J. Phys. Chem. B* **2006**, *110* (8), 3472–3476. <https://doi.org/10.1021/jp054556q>.
- (34) Bowron, D. T.; Finney, J. L.; Soper, A. K. Structural Investigation of Solute-Solute Interactions in Aqueous Solutions of Tertiary Butanol. *J. Phys. Chem. B* **1998**, *102* (18), 3551–3563. <https://doi.org/10.1021/jp972780c>.
- (35) Bowron, D. T.; Soper, A. K.; Finney, J. L. Temperature Dependence of the Structure of a 0.06 Mole Fraction Tertiary Butanol-Water Solution. *J. Chem. Phys.* **2001**, *114* (14), 6203–6219. <https://doi.org/10.1063/1.1354167>.
- (36) Hore, P. J. *Nuclear Magnetic Resonance*, Second.; Oxford University Press: Oxford, 2014.
- (37) Claridge, Timothy, D. W. *High-Resolution NMR Techniques in Organic Chemistry*, Third.; Elsevier: Oxford, 2016.
- (38) Lambert, J. B.; Mazzola, E. P. *Nuclear Magnetic Resonance Spectroscopy: An Introduction to Principles, Applications, and Experimental Methods*, First.; Pearson Education, Inc.: Upper Saddle River, 2004.
- (39) Maynard, A. J.; Sharman, G. J.; Searle, M. S. Origin of  $\beta$ -Hairpin Stability in Solution: Structural and Thermodynamic Analysis of the Folding of a Model Peptide Supports Hydrophobic Stabilization in Water. *J. Am. Chem. Soc.* **1998**, *120* (9), 1996–2007. <https://doi.org/10.1021/ja9726769>.
- (40) Qvist, J.; Halle, B. Thermal Signature of Hydrophobic Hydration Dynamics. *J. Am. Chem. Soc.* **2008**, *130* (31), 10345–10353. <https://doi.org/10.1021/ja802668w>.
- (41) Shimizu, A.; Fumino, K.; Yukiyasu, K.; Taniguchi, Y. NMR Studies on Dynamic Behavior of Water Molecule in Aqueous Denaturant Solutions at 25 °C: Effects of Guanidine Hydrochloride, Urea and Alkylated Ureas. *J. Mol. Liq.* **2000**, *85* (3), 269–278. [https://doi.org/10.1016/S0167-7322\(00\)00106-9](https://doi.org/10.1016/S0167-7322(00)00106-9).
- (42) Yoshida, K.; Ibuki, K.; Ueno, M. Pressure and Temperature Effects on  $^2\text{H}$  Spin-Lattice Relaxation Times and  $^1\text{H}$  Chemical Shifts in Tert-Butyl Alcohol- and Urea- $\text{D}_2\text{O}$  Solutions. *J. Chem. Phys.* **1998**, *108* (4), 1360–1367. <https://doi.org/10.1063/1.475509>.
- (43) Ohto, T.; Hunger, J.; Backus, E. H. G.; Mizukami, W.; Bonn, M.; Nagata, Y. Trimethylamine-N-Oxide: Its Hydration Structure, Surface Activity, and Biological Function, Viewed by Vibrational Spectroscopy and Molecular Dynamics Simulations. *Physical Chemistry Chemical Physics*. 2017, pp 6909–6920. <https://doi.org/10.1039/c6cp07284d>.
- (44) Ohtaki, H.; Radnai, T. Structure and Dynamics of Hydrated Ions. *Chem. Rev.* **1993**, *93* (3), 1157–1204. <https://doi.org/10.1021/cr00019a014>.
- (45) Van Der Maarel, J. R. C.; Lankhorst, D.; De Bleijser, J.; Leyte, J. C. Water Dynamics in Aqueous Electrolyte Solutions from Proton, Deuterium, and Oxygen-17 Nuclear Magnetic Relaxation. *J. Phys. Chem.* **1986**, *90* (7), 1470–1478. <https://doi.org/10.1021/j100398a050>.
- (46) Engel, G.; Hertz, H. On the Negative Hydration. A Nuclear Magnetic Relaxation Study. *Berichte der Bunsengesellschaft für Phys. Chemie* **1968**, *72* (7), 808–834.

- <https://doi.org/10.1002/bbpc.19680720713>.
- (47) Laage, D.; Stirnemann, G. Effect of Ions on Water Dynamics in Dilute and Concentrated Aqueous Salt Solutions. *J. Phys. Chem. B* **2019**, *123* (15), 3312–3324. <https://doi.org/10.1021/acs.jpcc.9b01053>.
- (48) Laage, D.; Stirnemann, G.; Sterpone, F.; Rey, R.; Hynes, J. T. Reorientation and Allied Dynamics in Water and Aqueous Solutions. *Annu. Rev. Phys. Chem.* **2011**, *62* (1), 395–416. <https://doi.org/10.1146/annurev.physchem.012809.103503>.
- (49) Endom, L.; Hertz, H. G.; Thül, B.; Zeidler, M. D. A Microdynamic Model of Electrolyte Solutions as Derived from Nuclear Magnetic Relaxation and Self-Diffusion Data. *Berichte der Bunsengesellschaft für Phys. Chemie* **1967**, *71* (9-10), 1008–1031. <https://doi.org/10.1002/bbpc.19670710907>.
- (50) Okouchi, S.; Moto, T.; Ishihara, Y.; Numajiri, H.; Uedaira, H. Hydration of Amines, Diamines, Polyamines and Amides Studied by NMR. *J. Chem. SOC. Faraday Trans.* **1996**, *92* (11), 1853–1857.
- (51) Bryant, R. G. THE DYNAMICS OF WATER-PROTEIN INTERACTIONS. *Annu. Rev. Biophys. Biomol. Struct.* **1996**, *25*, 29–53.
- (52) Ishihara, Y.; Okouchi, S.; Uedaira, H. Dynamics of Hydration of Alcohols and Diols in Aqueous Solutions. *J. Chem. Soc. - Faraday Trans.* **1997**, *93* (18), 3337–3342. <https://doi.org/10.1039/a701969f>.
- (53) Haselmeier, R.; Holz, M.; Marbach, W.; Weingärtner, H. Water Dynamics near a Dissolved Noble Gas. First Direct Experimental Evidence for a Retardation Effect. *J. Phys. Chem.* **1995**, *99* (8), 2243–2246. <https://doi.org/10.1021/j100008a001>.
- (54) Laage, D.; Elsaesser, T.; Hynes, J. T. Water Dynamics in the Hydration Shells of Biomolecules. *Chem. Rev.* **2017**, *117* (16), 10694–10725. <https://doi.org/10.1021/acs.chemrev.6b00765>.
- (55) Jasnin, M.; Moulin, M.; Haertlein, M.; Zaccari, G.; Tehei, M. Down to Atomic-Scale Intracellular Water Dynamics. *EMBO Rep.* **2008**, *9* (6), 543–547. <https://doi.org/10.1038/embor.2008.50>.
- (56) Persson, E.; Halle, B. Cell Water Dynamics on Multiple Time Scales. *Proc. Natl. Acad. Sci. U. S. A.* **2008**, *105* (17), 6266–6271. <https://doi.org/10.1073/pnas.0709585105>.
- (57) Laurent, H.; Soper, A. K.; Dougan, L. Trimethylamine: N -Oxide (TMAO) Resists the Compression of Water Structure by Magnesium Perchlorate: Terrestrial Kosmotrope vs. Martian Chaotrope. *Phys. Chem. Chem. Phys.* **2020**, *22* (9), 4924–4937. <https://doi.org/10.1039/c9cp06324b>.
- (58) Canchi, D. R.; García, A. E. Cosolvent Effects on Protein Stability. *Annu. Rev. Phys. Chem.* **2013**, *64* (1), 273–293. <https://doi.org/10.1146/annurev-physchem-040412-110156>.
- (59) Stejskal, E. O.; Tanner, J. E. Spin Diffusion Measurements: Spin Echoes in the Presence of a Time-Dependent Field Gradient. *J. Chem. Phys.* **1965**, *42* (1), 288–292. <https://doi.org/10.1063/1.1695690>.
- (60) Bowron, D. T.; Soper, A. K.; Jones, K.; Ansell, S.; Birch, S.; Norris, J.; Perrott, L.; Riedel, D.; Rhodes, N. J.; Wakefield, S. R. et al. NIMROD: The Near and InterMediate Range Order Diffractometer of the ISIS Second Target Station. *Rev. Sci. Instrum.* **2010**, *81* (3), 033905. <https://doi.org/10.1063/1.3331655>.
- (61) Soper, A. K. Tests of the Empirical Potential Structure Refinement Method and a New Method of Application to Neutron Diffraction Data on Water. *Mol. Phys.* **2001**, *99* (17), 1503–1516.

<https://doi.org/10.1080/00268970110056889>.

- (62) Soper, A. K. Empirical Potential Monte Carlo Simulation of Fluid Structure. *Chem. Phys.* **1996**, *202* (2–3), 295–306. [https://doi.org/10.1016/0301-0104\(95\)00357-6](https://doi.org/10.1016/0301-0104(95)00357-6).
- (63) Hammerich, A. D.; Buch, V. An Alternative Near-Neighbor Definition of Hydrogen Bonding in Water. *J. Chem. Phys.* **2008**, *128* (11), 111101. <https://doi.org/10.1063/1.2889949>.
- (64) Henchman, R. H.; Cockram, S. J. Water's Non-Tetrahedral Side. *Faraday Discuss.* **2013**, *167*, 529–550. <https://doi.org/10.1039/c3fd00080j>.
- (65) Prada-Gracia, D.; Shevchuk, R.; Rao, F. The Quest for Self-Consistency in Hydrogen Bond Definitions. *J. Chem. Phys.* **2013**, *139* (8), 084501. <https://doi.org/10.1063/1.4818885>.
- (66) Khan, A. A Liquid Water Model: Density Variation from Supercooled to Superheated States, Prediction of H-Bonds, and Temperature Limits. *J. Phys. Chem. B* **2000**, *104* (47), 11268–11274. <https://doi.org/10.1021/jp0016683>.
- (67) Kumar, R.; Schmidt, J. R.; Skinner, J. L. Hydrogen Bonding Definitions and Dynamics in Liquid Water. *J. Chem. Phys.* **2007**, *126* (20), 204107. <https://doi.org/10.1063/1.2742385>.
- (68) Matsumoto, M. Relevance of Hydrogen Bond Definitions in Liquid Water. *J. Chem. Phys.* **2007**, *126* (5), 054503. <https://doi.org/10.1063/1.2431168>.
- (69) Swiatla-Wojcik, D. Evaluation of the Criteria of Hydrogen Bonding in Highly Associated Liquids. *Chem. Phys.* **2007**, *342* (1–3), 260–266. <https://doi.org/10.1016/j.chemphys.2007.10.009>.
- (70) Bandyopadhyay, D.; Mohan, S.; Ghosh, S. K.; Choudhury, N. Correlation of Structural Order, Anomalous Density, and Hydrogen Bonding Network of Liquid Water. *J. Phys. Chem. B* **2013**, *117* (29), 8831–8843. <https://doi.org/10.1021/jp404478y>.
- (71) Ozkanlar, A.; Zhou, T.; Clark, A. E. Towards a Unified Description of the Hydrogen Bond Network of Liquid Water: A Dynamics Based Approach. *J. Chem. Phys.* **2014**, *141* (21), 214107. <https://doi.org/10.1063/1.4902538>.
- (72) Auer, B. M.; Skinner, J. L. Water: Hydrogen Bonding and Vibrational Spectroscopy, in the Bulk Liquid and at the Liquid/Vapor Interface. *Chem. Phys. Lett.* **2009**, *470* (1–3), 13–20. <https://doi.org/10.1016/j.cplett.2009.01.010>.
- (73) Mills, R. Self-Diffusion in Normal and Heavy Water in the Range 1–45°. *J. Phys. Chem.* **1973**, *77* (5), 685–688. <https://doi.org/10.1021/j100624a025>.
- (74) Graf, V.; Noack, F.; Béné, G. J. Proton Spin T1 Relaxation Dispersion in Liquid H<sub>2</sub>O by Slow Proton-Exchange. *J. Chem. Phys.* **1980**, *72* (2), 861–863. <https://doi.org/10.1063/1.439240>.
- (75) Stirnemann, G.; Wernersson, E.; Jungwirth, P.; Laage, D. Mechanisms of Acceleration and Retardation of Water Dynamics by Ions. *J. Am. Chem. Soc.* **2013**, *135* (32), 11824–11831. <https://doi.org/10.1021/ja405201s>.
- (76) Park, S.; Odellius, M.; Gaffney, K. J. Ultrafast Dynamics of Hydrogen Bond Exchange in Aqueous Ionic Solutions. *J. Phys. Chem. B* **2009**, *113* (22), 7825–7835. <https://doi.org/10.1021/jp9016739>.
- (77) Bakker, H. J. Structural Dynamics of Aqueous Salt Solutions. *Chem. Rev.* **2008**, *108* (4), 1456–1473. <https://doi.org/10.1021/cr0206622>.
- (78) Foster, R. J.; Damion, R. A.; Baboolal, T. G.; Smye, S. W.; Ries, M. E. A Nuclear Magnetic Resonance Study of Water in Aggregan Solutions. *R. Soc. Open Sci.* **2016**, *3* (3), 150705. <https://doi.org/10.1098/rsos.150705>.

- (79) Ezzawam, W. M.; Ries, M. E. Diffusion and Relaxometry to Study Carbohydrates Dissolved in Ionic Liquids. In *NMR Methods for Characterization of Synthetic and Natural Polymers*; Zhang, R., Sun, P., Eds.; Royal Society of Chemistry, 2019; pp 36–62.
- (80) Laage, D.; Hynes, J. T. A Molecular Jump Mechanism of Water Reorientation. *Science* **2006**, *311* (5762), 832–835. <https://doi.org/10.1126/science.1122154>.
- (81) Laage, D.; Hynes, J. T. On the Molecular Mechanism of Water Reorientation. *J. Phys. Chem. B* **2008**, *112* (45), 14230–14242. <https://doi.org/10.1021/jp805217u>.
- (82) Stirnemann, G.; Duboué-Dijon, E.; Laage, D. Ab Initio Simulations of Water Dynamics in Aqueous TMAO Solutions: Temperature and Concentration Effects. *J. Phys. Chem. B* **2017**, *121* (49), 11189–11197. <https://doi.org/10.1021/acs.jpcc.7b09989>.
- (83) Ball, P.; Hallsworth, J. E. Water Structure and Chaotropy: Their Uses, Abuses and Biological Implications. *Phys. Chem. Chem. Phys.* **2015**, *17* (13), 8297–8305. <https://doi.org/10.1039/c4cp04564e>.
- (84) Busch, S.; Pardo, L. C.; O'Dell, W. B.; Bruce, C. D.; Lorenz, C. D.; McLain, S. E. On the Structure of Water and Chloride Ion Interactions with a Peptide Backbone in Solution. *Phys. Chem. Chem. Phys.* **2013**, *15* (48), 21023. <https://doi.org/10.1039/c3cp53831a>.

### TOC Graphic

